DOI: 10.1002/ejic.200800702

Rhodium and Iridium Amino, Amido, and Aminyl Radical Complexes

Nicola Donati,[a] Daniel Stein,[a] Torsten Büttner,[a] Hartmut Schönberg,[a] Jeffrey Harmer,[b] Sreekanth Anadaram,[a] and Hansjörg Grützmacher*[a]

Keywords: Cyclic voltammetry / Iridium / Organometallic compounds / Phosphanes / Reaction mechanisms / Rhodium

The chlorido-bridged dimeric complex $[Rh_2(\mu\text{-}Cl)_2(trop_2NH)_2]$ [$trop_2NH$ = bis(benzo[*a*,*d*]cycloheptenyl)amine] or the acetonitrile complexes $[Rh(trop_2NH)(MeCN)_2]^+$ ($CF_3SO_3^-$) and [IrCl(MeCN)($trop_2NH$)] are well-suited precursor complexes for phenanthroline-type complexes [M(trop2NH)(R,R-phen)]$^+A^-$ (M = Rh, Ir; R = H, Me, Ph substituents in the 4,7- or 5,6-positions of the phen ligand, A^- = $CF_3SO_3^-$, PF_6^-). These complexes contain 18-valence-electron configured metal centers in a trigonal–bipyramidal coordination sphere with the amino (NH) group in an axial position and each of the olefinic C=C_{trop} units is in an equatorial position. The cationic amino complexes $[M(trop_2NH)(R,R\text{-}phen)]^+$ are sufficiently acidic (pK_a in dmso: 18.2–19.0) to be quantitatively deprotonated by one equivalent of KO*t*Bu to give neutral amido complexes $[M(trop_2N)(R,R\text{-}phen)]$ (M = Rh, Ir). These can be easily oxidized to give aminyl radical complexes $[M(trop_2N^{\cdot})(R,R\text{-}phen)]^+A^-$, which for M = Rh can be isolated as green crystals. The iridium complex $[Ir(trop_2N^{\cdot})(phen)]^+$ is unstable. High-resolution pulse EPR spectroscopy was used to gain insight into the electronic structure of the aminyl radical complexes. Remarkably, the rhodium and iridium complexes have a very similar electronic structure, as revealed by their EPR parameters {$[Rh(trop_2N^{\cdot})(phen)]^+$: $g_{1,2,3}$ = 2.084(2), 2.049(2), 2.027(2); $|A_{iso}|$ = 45.4 (N1), 10.4 (N2), 3.1 (N3) 27.0 (Rh) MHz; $[Ir(trop_2N^{\cdot})(phen)]^+$: $g_{1,2,3}$ = 2.140(2), 2.107(2), 2.015(2); $|A_{iso}|$ = 47 (N1), 7.9 (N2), 3.5 (N3), 26.8 (Ir) MHz} and these show that about 60 % of the spin population is localized on the nitrogen center (N1) of the $trop_2N$ ligand. In reactions with stannanes (R_3SnH) and thiols (RSH), H-atom transfer to the $trop_2N$ nitrogen atom is observed, $[M(trop_2N^{\cdot})(phen)]^+ + EH \rightarrow [M(trop_2NH)(phen)]^+ + 1/2HE\text{–}EH$.

Introduction

Aminyl radicals are short-lived intermediates that efficiently abstract hydrogen atoms from organic substrates or add to unsaturated bonds.[1] More persistent radicals can be obtained with π-conjugated, lone-pair carrying, and/or bulky substituents bonded to the nitrogen center. Also, metal fragments can stabilize aminyl radicals to an extent that they become detectable or even isolatable. Examples are shown in Scheme 1. It is a priori not always possible to properly assign the electronic state of such a complex, which can be formulated with two limiting resonance structures, [M]-($^{\cdot}NR_2$) (aminyl radical complex), or $[M^{+\cdot}]$-($^-NR_2$) (metal amide). Early examples are **A** and **B**, which were both discussed as aminyl radical complexes. On the basis of the EPR data, the unstable ($t_{1/2} \approx 90$ s at 25 °C in water) red-violet Ni^{II} complex **A**, obtained by deprotonation of a Ni^{III} amine precursor complex, was formulated with a macrocyclic aminyl radical as ligand.[2] In contrast, spectroscopic and computational data clearly show that **B**, isolatable as an blue-black microcrystalline powder, is a low-spin d^5 Mn^{II} complex with an amido ligand (no N^{14} hyperfine coupling could be observed).[3] The first compounds that were unambiguously characterized by a variety of spectroscopic techniques as aminyl radical complexes are the cobalt(III) anilino radical complex **C** and some related Mn^{IV} complexes with one, two, and three coordinated amilino radicals.[4] Complexes **D**–**G** could be isolated and were thoroughly investigated including structural analyses for **A**, **E**, and **G**.[5–8] With the exception of **E**, which is better described as a d^5 Ru^{III} amido complex with a relatively small portion of the spin population on the nitrogen center,[6] these complexes can be formulated as aminyl radical complexes; that is, the major part of the spin population resides on the N center.

A limited amount of data concerning the reactivity of aminyl radical complexes is available. Care must be taken when conclusions concerning the spin population are made. For example, on the one side, Mn^{II} amido complex **B** reacts as if it is an aminyl radical complex in the sense that H atoms are abstracted from the solvent or boranes to give the amine complex $[Mn(Cp)(CO)_2(NH_2R)]$.[3b] On the other side, Ru complex **E** with 8 % of the spin population ρ at the N center does indeed not show N-centered reactivity.[6] Complexes **D** (ρ_N = 57 %),[5] **G** (ρ_N = 57 %),[8] and **H** (ρ_N = 2 × 28 %),[9] which carry a substantial amount of spin den-

[a] Department of Chemistry and Applied Biosciences, ETH Zürich,
Wolfgang-Pauli Str. 10, 8093 Zürich, Switzerland
[b] CAESR, Inorganic Chemistry, University of Oxford,
South Parks Road, OX1 3QR, United Kingdom

Supporting information for this article is available on the WWW under http://www.eurjic.org or from the author.

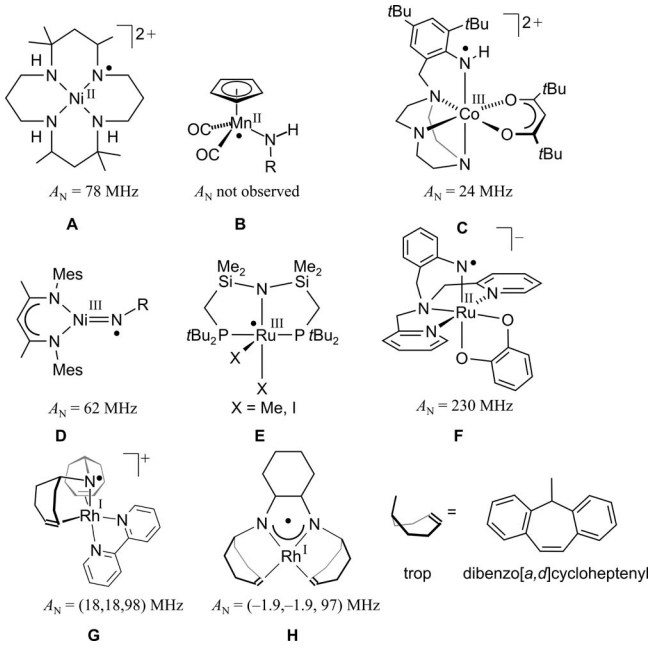

Scheme 1. Selected aminyl radical complexes.

sity at the nitrogen center, undergo the expected H-abstraction reactions leading to the corresponding amine complexes. Specifically, $[Rh(trop_2N^{\cdot})(bipy)]^+$ (**G**) (trop = benzo[*a,d*]cycloheptenyl) reacts rapidly with stannanes (R_3SnH) and thiols (RSH) to give $[Rh(trop_2NH)(bipy)]^+$ and $R_3Sn–SnR_3$ or RS–SR, respectively.

Ruthenium aminyl radical complexes related to **F** may serve as catalysts for the electrochemical oxidation of alcohols to carbonyls.[10] We reported that an iridium complex related to **H** is a very efficient catalyst for the chemoselective dehydrogenation of a wide range of primary alcohols to aldehydes in combination with *para*-benzoquinone as oxidant.[11] Curiously, rhodium complex **H** is inactive.

The motivation for the present study was to extend our understanding of the properties and reactivity of late-transition-metal aminyl radical complexes. We aimed at complexes of type **G** because this aminyl radical complex is remarkably stable, albeit reactive.[8] In this paper, we report a second complete set of a Rh^I amine, amido, and aminyl radical complexes of type **G** and the synthesis of the first analogous Ir^I aminyl radical complex. Furthermore, we describe in detail the synthesis of various rhodium and iridium $trop_2NH$ complexes.

Results

Syntheses

For the synthesis of $[Rh(trop_2NH)(L\cap L)]$ complexes ($L\cap L$ = bidentate ligand) two routes proved to be useful. The first one employs the chlorido-bridged dimer $[Rh_2(\mu\text{-}Cl)_2(trop_2NH)_2]$ (**3**) as a precursor,[12a,12b] which is easily obtained as red crystals by treating the commercially available cyclooctadiene (cod) complex $[Rh_2(\mu\text{-}Cl)_2(cod)_2]$ (**1**) with the amine $trop_2NH$ (**2**; Scheme 2). The other complex that serves as a precursor to $Rh(trop_2NH)$-type complexes[13,8] is the cationic bis(acetonitrile) complex $[Rh(trop_2NH)(MeCN)_2]OTf$ (**5**; OTf = $CF_3SO_3^-$). This complex is obtained in quantitative yield as yellow (micro) crystals either by treating **3** in acetonitrile with AgOTf or by treating the bis(cod) complex $[Rh(cod)_2]OTf$ with amine **2** in acetonitrile. Both **3** and **5** can be stored at ambient temperature in closed vessels for years without signs of decomposition.

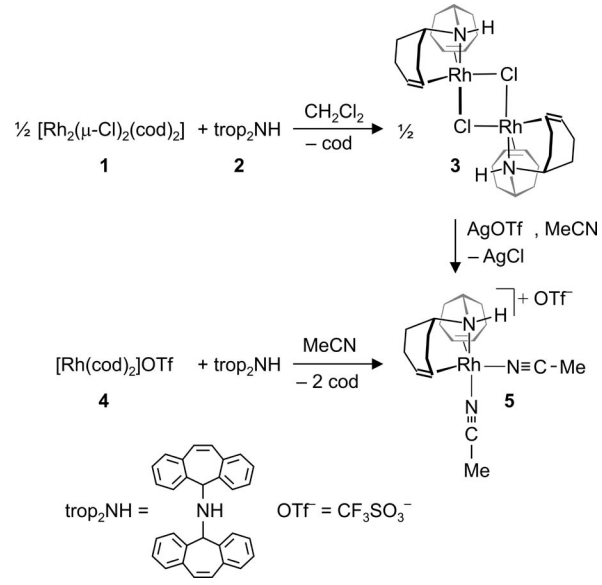

Scheme 2. Syntheses of precursor complexes **3** and **5**.

A CD_3CN solution of $[Rh(trop_2NH)(MeCN)_2]OTf$ (**5**) shows two sharp and distinct resonances for coordinated MeCN [$\delta(^1H)$ = 2.4 ppm] and one uncoordinated MeCN molecule [$\delta(^1H)$ = 1.96 ppm]. We assign the first resonance to the kinetically inert axial bonded MeCN in **5**, whereas the MeCN molecule in the equatorial position is labile and displaced by the CD_3CN solvent molecules.[14]

The syntheses leading to complexes **6a**–**d** with phenanthroline (phen) and its derivatives ^{R}phen as ligands is displayed in Scheme 3. Complex **6a** is simply prepared by treating phen with chlorido-bridged dimer **3** in the presence of AgOTf in boiling thf. For the complexes carrying the substituted phenanthroline derivatives, bis(acetonitrile) complex **5** proved to be the better precursor. All complexes **6a**–**d** were obtained as stable yellow to bright orange (micro)crystalline powders in good isolated yields (≈80%).

Neutral acetylacetonate (acac) complex **7** was prepared from $[Rh_2(\mu\text{-}Cl)_2(trop_2NH)_2]$ and acetylacetone (Hacac) in the presence of KO*t*Bu as base.

The synthesis of the iridium phenanthroline complex $[Ir(trop_2NH)(phen)]PF_6$ (**11**) requires harsher reaction conditions. First, the yellow dimeric species $[Ir_2(\mu\text{-}Cl)_2(trop_2NH)_2]$ (**9**) was prepared in moderate yield by treating the cyclooctene (coe) complex $[Ir_2(\mu\text{-}Cl)_2(coe)_4]$ with $trop_2NH$ in boiling toluene for 2 d. This complex cannot be converted directly into **11** in a similar manner, as found for

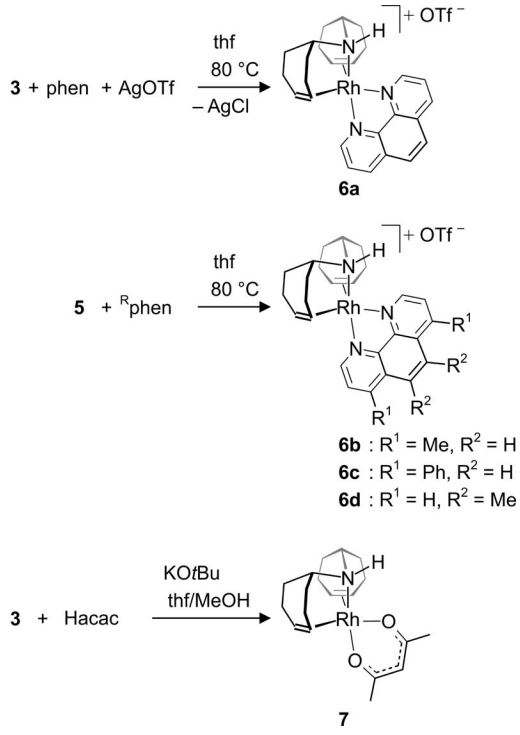

Scheme 3. Syntheses of amine olefin phenanthrolin complexes **6a**–**d** and acetylacetonato complex **7**.

the analogous rhodium complex. Instead, **9** needed to be converted into mono(acetonitrile) complex **10**. This complex is also obtained when the cycooctadiene complex $[Ir_2(\mu\text{-}Cl)_2(cod)_2]$ is treated with $trop_2NH$ (**2**) in acetonitrile as solvent (not included in Scheme 4). Finally, when colorless complex **10** was dissolved in chlorobenzene in the presence of phen and $TlPF_6$, a deep-red solution was obtained that turns into a bright orange suspension after heating at reflux overnight. Desired product **11** could be obtained in high yield (>90%) as a yellow powder.

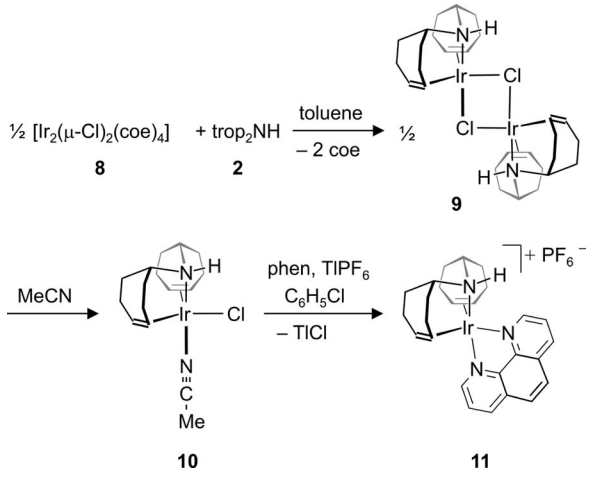

Scheme 4. Syntheses of iridium complexes **9**–**11**.

The rhodium complexes with phen (**6a**), 4,7-dimethylphenanthrolin (**6b**), and 4,7-diphenylphenanthroline (**6c**) as ligands can be quantitatively deprotonated to the corresponding neutral amido complexes **12a**–**c** by using one equivalent of KO*t*Bu as base in thf as solvent. Neutral complex **7**, however, did not react to identifiable products under the same reaction conditions. Iridium complex **11** is again quantitatively deprotonated by one equivalent of KO*t*Bu to give neutral iridium amido complex **13**. All amido complexes can be isolated as red (**12a**), red-brown (**12b**,**c**), or green-brown (**13**) air-sensitive microcrystalline powders (see Scheme 5).

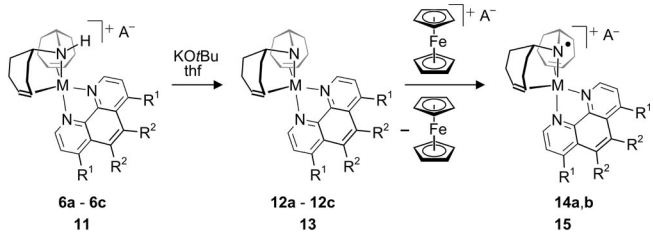

A⁻ = OTf^- or PF_6^-

	M	R^1	R^2
6a , **12a**, **14a**	Rh	H	H
6b , **12b**, **14b**	Rh	Me	H
6c , **12c**	Rh	Ph	H
11 , **13**, **15**	Ir	H	H

Scheme 5. Syntheses of amido complexes **12a**–**13** and aminyl radical complexes **14a**,**b** and **15**.

From the radical cation complexes obtained by chemical oxidation of amido complexes **12a**,**b** (M = Rh) or **13** (M = *I*r) with ferrocenium triflate in thf, compounds **14a** and **14b** were isolated as dark-green powders after precipitation with *n*-hexane. From a concentrated solution, dark-red single crystals of **14a** were obtained. Despite many attempts, iridium analogue **15** could not be isolated. This compound rapidly decomposes and can only be characterized by EPR spectroscopy (vide infra).

NMR Spectroscopic Data

Selected ^{13}C and ^{1}H NMR spectroscopic data of complexes **3**, **5**, **6a**–**d**, **7**, **9**–**11**, **12a**–**c**, and **13** are listed in Table 1 and are in accord with C_s-symmetric structures. The NMR spectroscopic data for phenanthroline complexes **6a** and **12a** are very similar to the reported data for the 2,2′-bipyridine complexes [Rh(trop$_2$NH)(bipy)]OTf[8] and [Rh(trop$_2$N)(bipy)]. A significant low-frequency coordination shift of the olefinic ^{13}C resonances {M = Rh: 60–67 ppm, M = Ir 77–86 ppm with respect to **2** [δ ($^{13}C_{ol}$) ≈ 130 ppm]} indicates significant back bonding and tight binding. The resonance of the acidic NH proton is sensitively influenced by the solvent and is shifted to higher frequencies in [D_6]-dmso (>5 ppm) relative to that in CD_3CN, [D_8]thf, or $CDCl_3$. The deprotonation of the NH group of cationic rhodium complexes **6a**–**c** or that of iridium complex **11** has a relatively small effect on the $^{13}C_{ol}$ resonances indicating no significant alteration of the M→L back donation in the amido complexes. The deprotonation has an effect on the ^{103}Rh resonances, which are shifted by about 500 ppm to lower frequencies in the amido complexes.

Table 1. Selected physical data for complexes **3**, **5**, **6a–d**, **7**, **9–11**, **12a–c**, and **13**. Chemical shifts are given on the δ scale in ppm, the redox potentials ($E°_{1/2}$) were referenced against the Fc^+/Fc couple and are given in V, and the bond dissociation energies (BDE) in kJ mol^{-1}. All data were obtained in dmso as solvent. n.d. = not determined; n.r. = not resolved.

Compound	Metal	Solvent	δ olefinic H[a]/H[b]	δ olefinic ^{13}C	δ NH	pK_a	$E°_{1/2}$	BDE	δ ^{103}Rh
3	Rh	CD_2Cl_2	5.97/6.20	71.4 (n.r.)	2.90	n.d.	n.d.	n.d.	2992
5	Rh	CD_3CN	5.36/5.77	70.3/71.0	4.03	n.d.	n.d.	n.d.	2311
6a	Rh	[D$_6$]dmso	3.99/5.56	68.0/69.3	5.04	18.6(2)	n.d.[a]	361(2)	2111
6b	Rh	CD_3CN	4.04/5.50	67.9/69.2	3.79	19.0(2)	n.d.	361(2)	2099
6c	Rh	[D$_6$]dmso	4.13/5.59	67.6/69.1	5.17	18.7(2)	n.d.	361(2)	2096
6d	Rh	CD_3CN	4.07/5.54	68.0/69.5	3.83	n.d.	n.d.	n.d.	2093
7	Rh	$CDCl_3$	4.83/5.19	66.8/69.9	2.92	n.d.	n.d.	n.d.	2998
9	Ir	$CDCl_3$	5.58/5.83	51.1/52.6	3.67	n.d.	n.d.	n.d.	–
10	Ir	$CDCl_3$	4.48/5.00	45.6/53.7	4.40	n.d.	n.d.	n.d.	–
11	Ir	[D$_8$]thf	3.26/5.18	47.9/51.1	4.78	18.2(1)	n.d.	353(1)	–
12a	Rh	[D$_8$]thf	2.73/4.81	63.3/64.1	–	–	–0.541	–	1570
12b	Rh	[D$_8$]thf	3.45/5.01	64.3/67.3	–	–	–0.568	–	1547
12c	Rh	[D$_6$]dmso	3.55/5.12	65.3/66.9	–	–	–0.544	–	1562
13	Ir	[D$_8$]thf	2.72/4.81	44.0/50.8	–	–	–0.602	–	–

[a] The redox potential measured in thf was –0.636 V. Cyclic voltammograms were recorded for the related 2,2′-bipyridine (bipy) complex [Rh(trop$_2$NH)(bipy)]OTf[8] in a thf/*n*Bu$_4$NPF6 electrolyte: $E°^1_{1/2}$ = +0.588 V (Rh^I/Rh^{II}); $E°^2_{1/2}$ = –1.77 V/Rh^I(bipy)/Rh^I(bipy$^-$).

Determination of the pK_a of 6a–c and 11

Dimethyl sulfoxide is widely used as nonprotic solvent for the determination of the pK_a of a wide range of organic substrates.[15] This solvent is a sufficiently strong solvent in order to suppress ion pairing, which otherwise renders the determination of pK_a values rather difficult. A serious drawback with organometallic complexes is that dmso might act as a ligand, and especially, it can displace weakly bound ligands from the metal center. However, this was not detected with saturated 18-electron complexes **6a–c** and **11**, and the pK_a of the coordinated amino group could be easily determined by using ^{1}H NMR spectroscopy. The pK_a of the sample complex $[M(NH)]^+$ is obtained through Equation (1).

$$pK_a[M(NH)] = pK_a(Href) - \log K \quad (1)$$

$$[M(NH)]^+ + ref^- \rightarrow [M(N)] + Href \quad (2)$$

where pK_a(Href) is the known pK_a value of a reference system in the same solvent, Href $\leftrightarrows$ H^+ + ref$^-$, and K is the equilibrium constant of the reaction given in Equation (2). K is determined by measuring suitable ^{1}H resonances of $[M(NH)]^+/[M(N)]$ and ref$^-$/Href. In order to obtained exact data, it is best to use a reference base that has a pK_a value very close to that expected for the sample. In this case, all species participating in the Equation (2) have almost equal concentrations, and the experimental error in the integration of the peak intensities is smallest. We found that the imidazolide/imidazole reference pair [pK_a(dmso) = 18.6(1)] is ideally suited for the determination of the pK_a of rhodium complexes **6a**,**b** and iridium complex **11**, whereas diacetamide/diacetamine (no proton resonances in the aromatic region) allowed the determination of the pK_a of **6c**. The pK_a data are listed in Table 1. The NH acidities lie in a narrow range of pK_a = 18.2–19.0 and compare well with the value determined for the analogous bipy complex [Rh(trop$_2$NH)(bipy)]OTf (pK_a = 18.7).[8] The pK_a of the coordinated trop$_2$NH ligand in the cationic 18-electron bis(amino)tris(olefin) complex [Rh(trop$_2$NH)(tropNH$_2$)]OTf is higher [pK_a = 20.6(1)].[13] Remarkably, the pK_a of the iridium complex [Ir(trop$_2$NH)(phen)]OTf (**11**) is almost the same as in the analogous rhodium species **6a**. This is in contrast to the observation we made for the tetracoordinate 16-electron bis(amino) complexes $[M(trop_2dach)]^+$ of type **H** (see Scheme 1), where the iridium complex has a pK_a value (pK_a^1 = 10.5; pK_a^2 = 19.6) about five orders of magnitude lower than that of the rhodium complex (pK_a^1 = 15.7; p$K_a^2 > 21$).[9,16] In addition, we looked into the rates of the deprotonation reactions of rhodium amine complex **6a** by using either imidazolide (Imd$^-$) as base [Equation (3)] or by inspection of the self-exchange reaction given in Equation (4).

$$\underset{\mathbf{6a}}{[Rh(trop_2NH)(phen)]^+} + Imd^- \leftrightarrows \underset{\mathbf{12a}}{[Rh(trop_2N)(phen)]} + HImd \quad (3)$$

$$\underset{\mathbf{6a}}{[Rh(trop_2N\mathit{H})(phen)]^+} + \underset{\mathbf{12a}}{[Rh(trop_2N)(phen)]} \leftrightarrows \underset{\mathbf{12a}}{[Rh(trop_2N)(phen)]} + \underset{\mathbf{6a}}{[Rh(trop_2N\mathit{H})(phen)]} \quad (4)$$

In the first case, the ^{1}H NMR spectrum at T = 298 K of a 1:1 mixture of **6a** and $Li^+(Imd^-)$ shows averaged sharp signals for the pairs $[Rh(trop_2NH)(phen)]^+/[Rh(trop_2N)(phen)]$ and Imd$^-$/HImd. Upon cooling, only a very small line-broadening effect for characteristic NMR resonances [i.e., the olefinic and benzylic ^{1}H resonances of the trop unit and the *H*C(N$_2$) proton of the imidazole] could be observed in the accessible temperature range between 230 and 298 K. The reaction given in Equation (3) remains fast on the NMR timescale, and we estimate a rate of $k_{obs} \approx 0.5–1 \times 10^6$ s^{-1}. The NMR spectra of a mixture of [Rh(trop$_2$NH)(phen)]OTf (**6a**) and [Rh(trop$_2$N)(phen)] (**12a**) show broad signals at T = 283 K that sharpen signifi-

cantly upon cooling to T = 213 K meaning that this process is rather slow on the NMR timescale. Line-shape analysis by using the MEXICO program package[17] allowed us to determine the activation barrier $\Delta G^{\#}_{298}$ = 67(1) kJ mol^{-1} and the rate of self-exchange for the reaction give in Equation (4): k = 11.2 s^{-1}.

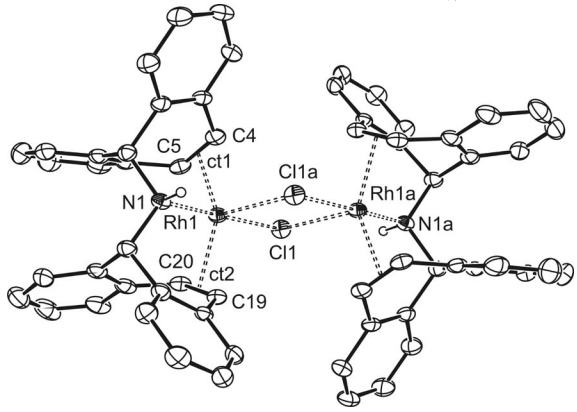

Figure 1. Molecular structure of **3**·$(CH_2Cl_2)_2$. The thermal ellipsoids correspond to 30% probability. The hydrogen atoms except at the nitrogen atoms and CH_2Cl_2 molecules are omitted for clarity. Selected bond lengths [Å] and angles [°]: Rh1–N1 2.076(5), Rh1–Cl1 2.384(2), Rh1–Cl1a 2.626(2), Rh–C4 2.165(5), Rh1–C5 2.145(6), Rh–C19 2.141(6), Rh–C20 2.165(6), Rh1–ct1 2.032(6),Rh1–ct2 2.032(6), C4–C5 1.435(8), C19–C20 1.421(8); N1–Rh1–Cl1 177.1(1), N1–Rh1–Cl1A 91.1(1), N1–Rh1–C5 91.1(1), ct1–Rh1–ct2 136.7(2); ct = centroid of the (C=Ctrop) bond.

Cyclic Voltammetry

The cyclic voltammogram (CV) of the previously reported cationic 2,2′-bipyridine (bipy) complex [Rh(trop$_2$NH)(bipy)]OTf[8] in a thf/nBu$_4$NPF$_6$ electrolyte shows a reversible redox wave at $E°_{1/2}$ = –1.77 V (vs. Fc$^+$/Fc). This reduction is ligand centered and leads to the neutral complex [Rh^{I}(trop$_2$NH)(bipy$^{\cdot-}$)]. We were unable to isolate this compound, but the formation of the bipy$^{\cdot-}$ radical anion is clearly proven by its characteristic EPR spectrum.[18,19] A quasireversible redox wave is observed at $E°_{1/2}$ = +0.588 V (vs. Fc$^+$/Fc). It is likely that this oxidation is a metal-centered process giving rhodium(II) complex [Rh^{II}(trop$_2$NH)(bipy)]$^{2+}$.[20] We were unable to isolate this complex or characterize it by EPR spectroscopy. In comparison to this cationic complex, neutral rhodium amido complexes **12a**–**c** and iridium amide **13** show markedly different cyclic voltammograms. All compounds are easily oxidized and show a reversible redox wave in a narrow range between –0.51 and –0.60 V (in dmso, vs. Fc$^+$/Fc). As discussed below, this oxidation is best described as ligand centered leading to an aminyl radical complex [M(trop$_2$N$^{\cdot}$)(N∩N)]$^+$. With the equation BDE = 5.74pK_a + 96.5$E°_{1/2}$ + C, which has been extensively used by Bordwell et al.[21] for the determination of the bond dissociation energies (BDEs) of organic compounds (C is an empirically derived constant of 306.9 kJ mol^{-1} in dmso), the NH dissociation energy for Rh^{I} complexes **6a**–**c** and Ir^{I} complex **11** is estimated to be 361(2) and 353(2) kJ mol^{-1}, respectively (Table 1). All data resemble closely those obtained for the [Rh(trop$_2$NH)(bipy)]$^+$/[Rh(trop$_2$N)(bipy)] couple [pK_a = 18.7(2); $E°_{1/2}$ = –0.552 V; BDE = 361(2) kJ mol^{-1}].[8]

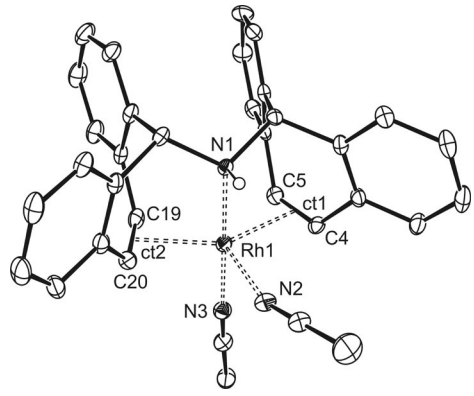

Figure 2. Structure of **5**. The thermal ellipsoids are drawn at 30% probability. The counteranion OTf$^-$ and all hydrogen atoms except at N1 are omitted for clarity. Selected bond lengths [Å] and angles [°]: Rh1–N1 2.075(3); Rh1–N2 2.191(4); Rh1–N3 2.007(4); Rh1–C4 2.185(4); Rh1–C5 2.169(4); Rh1–C19 213.5(4); Rh1–C20 2.140(5) Rh1–ct1 2.060(6), Rh1–ct2 2.199(6), C4–C5 1.411(6), C19–C20 1.417(6); N1–Rh1–N3 178.1(2); N1–Rh1–N2 87.0(1); N2–Rh1–ct(C4,C5) 105.4(2), N2–Rh1–ct(C19,C20) 117.7(2); ct = centroid of the (C=C$_{trop}$) bond.

Structures from X-ray Diffraction Data

The structures of **3**, **5**, **7**, **6a**,**d**, **12a**, and **14a** were determined by X-ray diffraction studies. Plots of the structures of **3**, **5**, **7**, and **14a** are shown in Figures 1, 2, 3, and 4, respectively. Selected bond lengths and angles for **3**, **5**, and **7** are given in the Figure captions. For **6a**,**d**, **12a**, and **14a**, selected distances and angles are listed in Table 2. Tables 4 and 5 contain information concerning the data collection and refinement of the examined structures.

In all complexes, the rhodium centers reside in mildly distorted trigonal bipyramidal (TBP) coordination spheres with the largest deviation seen in the ct–Rh–ct angles, which are >130° (ideally 120°). In the idealized structures, the trop units are related by mirror symmetry; complex **5** has, in addition, a center of inversion within the planar R_2Cl_2 ring. With the exception of **14a** (vide infra), the Rh–N1 bond is longer than 2 Å (2.046 Å in **12a** to 2.088 Å in **6a**). The distances from the Rh center to the centroids (ct) of the coordinated C=C$_{trop}$ units do not vary greatly (2.003 Å

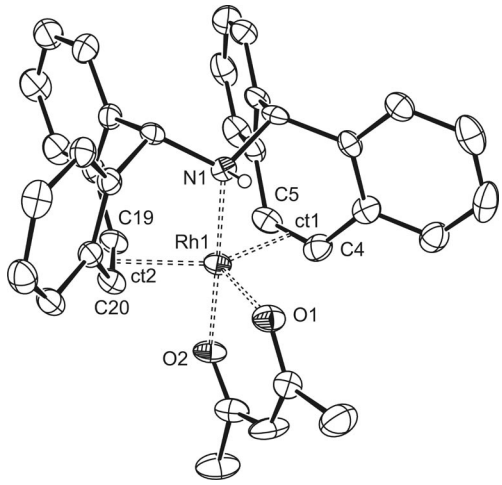

Figure 3. Structure of **7**·CH_2Cl_2. The thermal ellipsoids are drawn at 30% probability. All hydrogen atoms except at N1 and the CH_2Cl_2 molecule are omitted for clarity. Selected bond lengths [Å] and angles [°]: Rh–N1: 2.059(5), Rh–O1: 2.185(4), Rh–O2 2.022(4), Rh1–C4 2.149(7); Rh1–C5 2.153(6); Rh1–C19 2.134(6); Rh1–C20 2.119(6) Rh1–ct1 2.031(6), Rh1–ct2 2.003(6), C4–C5 1.418(9), C19–C20 1.424(8); N1–Rh1–O2 178.95(2); N1–Rh–O1 87.66(2); O1–Rh–O2 92.74(2); ct1–Rh–ct2 137.4(2); ct = centroid of the C=C bond.

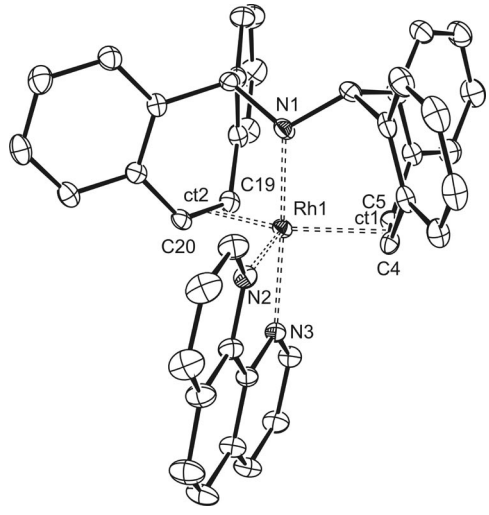

Figure 4. The structure of aminyl radical cation complex $[Rh(trop_2N^{\cdot})(phen)]^+$ (**14a**) is shown as an example (thermal ellipsoids at 30% probability) and indicates the atom labeling scheme used for all compounds. The structures of **6a**,**d** and **12a** are not displayed. N1 represents an NH function in **6a**,**d**, an amide nitrogen in **12a**, and an aminyl center in **14a**. Selected bond lengths [Å] and angles [°] for all compounds are given in Table 2. ct = centroid of the C=C bond.

in **7** to 2.199 Å in **5**), and neither do the coordinated $C{=}C_{trop}$ bond lengths, which are about 1.42 Å on average (the C=C bond in the free $trop_2NR$ ligands is about 1.34 Å).[18] The elongation of the coordinated $C{=}C_{trop}$ bonds (>1.41 Å) indicate considerable M→L back donation and tight binding. In agreement with the NMR spectroscopic data, the structural data also suggest that the M→L back donation is only slightly influenced by the nature of the different chelate ligands or the deprotonation of the NH group. A further common feature of all complexes is that, as expected, the labile σ donor (Cl in **3**; MeCN in **5**; O in **7**; N in **6a**,**d**, **12a**, and **14a**) in the equatorial position of the TBPs around each Rh center is bound at significantly longer distances than that found for the corresponding ligand in the axial position.

With complexes **6a**, **12a**, and **14a**, respectively, a second complete series of amino, amido, and aminyl radical complexes could be structurally investigated. The data listed in Table 2 are very close to those we obtained for the series of 2,2′-bipyridine complexes $[Rh(trop_2NX)(bipy)]^n$ (X = H, n = +1; X = lone pair, n = 0; X = ·, n = +1).[8] As we observed in this series, the only significant structural change occurs when neutral amido complex **12a** is oxidized to radical cation complex **14a**. In this complex, the Rh1–N1 bond [1.947(4) Å] is significantly shorter than that in all other compounds. Furthermore, the sum of the bond angles around N1, Σ°(N1), flattens and is close to 360°, whereas in all other complexes Σ°(N1) is closer to 340°, also in amido complex **12a**. The shortening of the Rh–N bond and the flattening of the N1 coordination sphere can be explained under the assumption that the removed electron resides in a Rh–N antibonding orbital.

EPR Spectroscopy

In order to gain further insight into the electronic structures, the aminyl radical complexes $[Rh(trop_2N^{\cdot})(phen)]OTf$ (**14a**) and its iridium analogue **15** were investigated with continuous wave (CW) and high-resolution pulse EPR methods.[22] Well-resolved CW EPR spectra of $[Rh(trop_2N^{\cdot})(phen)]OTf$ (**14a**) were obtained in a thf/acetone (2:1 by vol.) solvent mixture at S-band and T = 298 K, as shown in Figure 5A. Couplings to one rhodium (I = 1/2), two nitrogen (I = 1), and two hydrogen nuclei (I = 1/2) are resolved. The isotropic hyperfine coupling constants listed in Table 3 were obtained through the simulation.

Table 2. Selected bond lengths [Å] and angles [°] for **6a**·$(thf)_2$, **6d**·CH_3CN, **12a**·$(thf)_2$, and **14a**·$(thf)_2$.

	Rh–N1	Rh–N2	Rh–N3	Rh-ct1	Rh-ct2	C=Ctrop	Σ°(N1)	N1–Rh–N3	ct1–Rh–ct2	N1–Rh–N2	N2–Rh–N3
6a·$(thf)_2$	2.088(2)	2.177(2)	2.033(2)	2.034(2)	2.021(2)	1.424(3)	343.2(1)	175.2(1)	134.8(1)	95.8(1)	79.4(1)
6d·CH_3CN	2.086(4)	2.193(3)	2.046(4)	2.060(5)	2.047(5)	1.427(7)	344.6(7)	175.2(2)	132.6(2)	97.2(2)	78.1(2)
12a·$(thf)_2$	2.046(1)	2.148(1)	2.099(1)	2.018(1)	2.020(1)	1.433(2)	342.3(1)	170.9(1)	136.4(1)	92.6(1)	78.3(1)
14a·$(thf)_2$	1.947(4)	2.188(4)	2.092(3)	2.084(4)	2.032(4)	1.417(6)	356.7(2)	177.3(2)	140.9(2)	102.1(2)	77.7(2)

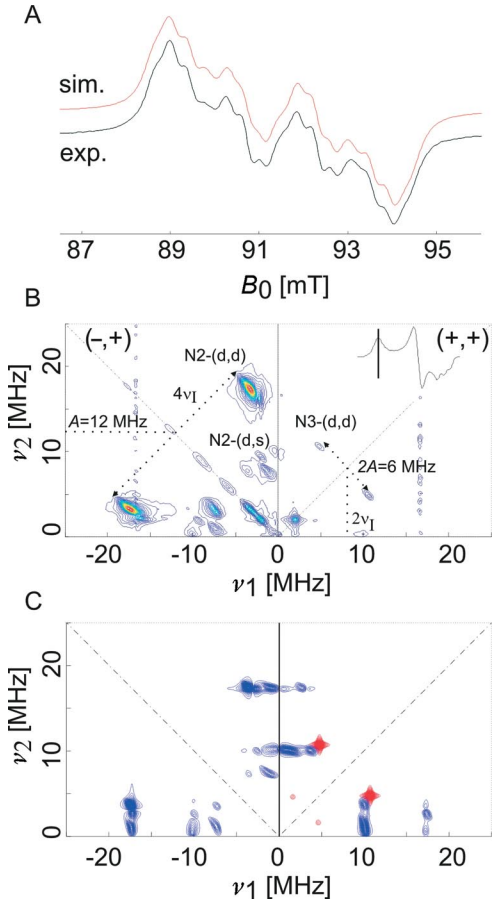

Figure 5. (A) S-band (2.63 GHz) CW EPR spectrum recorded at room temperature (298 K) of **14a** in thf/acetone (2:1). Experimental (exp.) and simulated (sim.) spectra. (B) Q-band (35.3 GHz) HYSCORE spectra of **14a** in thf measured at 25 K at observer positions B_0 = 1220.9 mT. Selected crosspeaks are assigned to nitrogen N1, N2, and N3 with labels for nitrogen double-quantum (d) and single-quantum (s) frequencies. Inset: Q-band echo-detected EPR spectrum (first derivative representation) showing the observer position used to record the HYSCORE spectrum. (C) Simulated Q-band HYSCORE spectrum.

The principal values of the rhombic g matrix [g_1 = 2.084(2), g_2 = 2.049(2), g_3 = 2.027(2)] and the large nitrogen hyperfine coupling of 100 MHz along g_3 were determined from echo-detected EPR frozen solution spectra at Q-band (see inset in Figure 5B) and W-band (not shown here). Pulse EPR techniques were applied to obtain a complete picture of the anisotropic part of the hyperfine interactions and thus the spin populations. As an example, a Q-band HYSCORE (hyperfine sublevel correlation) spectrum of **14a** measured at T = 25 K is shown in Figure 5B along with its simulation (Figure 5C).

At the chosen observer position of B_0 = 1220.9 mT (indicated by the line position in the EPR spectrum displayed in the inset of Figure 5B), crosspeaks from the nitrogen nuclei N2 (strong coupling case $|A| > 2|\nu_{14N}|$) in the (–,+) quadrant and N3 (weak coupling case $|A| < 2|\nu_{14N}|$) in the (+,+) quadrant are observed. The position of the double-quantum crosspeaks allow initial guesses for the hyperfine couplings (for a small quadrupole interaction), as they are centered at the hyperfine value A and split by $4\nu_{14N}$ in the strong coupling case, and in the weak coupling case the double-quantum peaks are centered at $2\nu_{14N}$ and split by $2A$ (Figure 5B). Measurements at several observer positions allowed determination of the principal values of the nitrogen hyperfine and nuclear quadrupole tensors listed in Table 3. The rhodium hyperfine principal values were obtained from the room-temperature and frozen-solution CW EPR spectra (see Supporting Information) recorded at X-band.

A paramagnetic iridium aminyl radical complex was significantly more difficult to stabilize. When the amide complex [Ir(trop$_2$N)(phen)] (**13**) was treated with a ferrocenium salt as oxidant under conditions identical to those used for the generation of **14** (solutions of which are stable at room temperature for at least a couple of weeks) no EPR signal could be detected and the NMR spectra showed resonances for the amine complex [Ir(trop$_2$NH)(phen)]$^+$ (**11**). Only when stock solutions of the amide [Ir(trop$_2$N)(phen)] and the ferrocenium salt were combined and the reaction mix-

Table 3. Hyperfine and nuclear quadrupole parameters for aminyl radical complexes **14a** and **15**. Numbers in brackets are error estimates.

[Rh(trop$_2$N$^{\cdot}$)(phen)]OTf (**14a**)			$g_{1,2,3}$ = 2.084(2), 2.049(2), 2.027(2)	
Nucleus	$\lvert A_{iso}\rvert$ [MHz]	$\lvert A_{1,2,3}\rvert$ [MHz]	$\lvert\kappa\rvert^{[a]}$ [MHz]	$\eta^{[a]}$
N1	45.4(5)	18(5), 18(5), 100(3)	1.6(2)	0.7(2)
N2	10.4(5)	12.3(5), 9.6(5), 8.7(5)	3.0(2)	0.3(1)
N3	3.1(2)	3.0(2), 3.2(2), 3.0(2)	2.6(2)	0.2(1)
Rh	27.0(5)	48(2), 16(3), 16(3)	–	–
H^{bz}(×2)	9.9(5)	–	–	–
[Ir{trop$_2$N$^{\cdot}$(phen)}] (OTf/PF$_6$) (**15**)			$g_{1,2,3}$ = 2.140(2), 2.107(2), 2.015(2)	
Nucleus	$\lvert A_{iso}\rvert$ [MHz]	$\lvert A_{1,2,3}\rvert$ [MHz]	$\lvert\kappa\rvert^{[a]}$ [MHz]	$\eta^{[a]}$
N1	47(5)	21(5), 21(5), 100(3)	1.5(2)	0.7(2)
N2	7.9(5)	10.2(5), 7.9(5), 5.7(5)	2.1(2)	0.0(1)
N3	3.5(5)	3.2(2), 4.0(2), 3.2(2)	2.2(2)	0.0(1)
^{191}Ir	26.8(5)	44(5), 30(5), <20	–	–

[a] Nuclear quadrupole interactions $\kappa = |e^2qQ/h|$ and asymmetry parameter $\eta = (Q_x - Q_y)/Q_z$ with $Q_x = -\kappa(1 - \eta)/[4I(2I - 1)]$, $Q_y = -\kappa(1 + \eta)/[4I(2I - 1)]$ and $Q_z = 2\kappa/[4I(2I - 1)]$.

ture rapidly frozen in liquid nitrogen could an EPR spectrum of **15** be recorded. Remarkably, the stability of **15** is significantly enhanced when a solution contains 10–25 mM of the iridium complex and about 400 mM of nBuN$_4$PF$_6$ as electrolyte. Under these circumstances, solutions of **15** remain EPR active for a couple of hours at room temperature. A frozen-solution (T = 120 K) CW EPR spectrum of **15** at X-band (9.53 GHz) is shown in Figure 6A, along with a satisfactory simulation obtained by employing the three principal g values and hyperfine couplings from the iridium nucleus and the N1 and N2 nuclei (two and three principal values were determined independently by HYSCORE data).[23] In addition, HYSCORE spectra taken at different observer positions (for an example see Figure 6B) enabled the determination of the complete set of hyperfine coupling constants of N1, N2, and N3 (see Table 3). As a result, we found a remarkable similarity between the spin population distribution in rhodium and iridium radical complexes **14** and **15**. Moreover, the ligand hyperfine coupling constants of both species are almost identical to that of the previously investigated bipyridine complex [Rh(trop$_2$N$^{\cdot}$)(bipy)]$^+$ (**G**; Scheme 1).[8] From the isotropic (A_{iso} = (2$A_{1,2}$ + A_3)/3) and dipolar (T = |$A_{1,2}$ – A_{iso}|) parts of the axial hyperfine interaction, the spin population for the N1 nucleus of the rhodium complex in the 2s orbital is calculated as 45.3/1443.9 MHz = 3.1% and for the 2p orbital 27.3/49.8 MHz = 55% (1443.9 and 49.8 MHz are the hyperfine coupling constant for ^{14}N with 100% spin population in the 2s and 2p orbital, respectively). For the iridium complex, the analysis of the N1 hyperfine coupling gives 3.3% (2s orbital) and 53% (2p orbital).

The hyperfine coupling of N1 with a large isotropic and a pronounced axial dipolar part, and the rather small anisotropy of the g matrix characterize these species best as Rh^{I} or Ir^{I} aminyl radical complexes with an estimated spin population of about 60% at the aminyl radical center N1. A DFT calculation that we performed for the bipy complex [Rh(trop$_2$N$^{\cdot}$)(bipy)]OTf (**G**) showed that the majority (≈30%) of remaining spin population is localized at the metal center.[8] Because the EPR spectra are very similar for **H**, **14a**, and **15**, we assume that in the latter the spin density at the metal center is of the same magnitude. In summary the results show that the M^{II} amide resonance form contributes significantly to the electronic ground state and stabilizes the complexes.

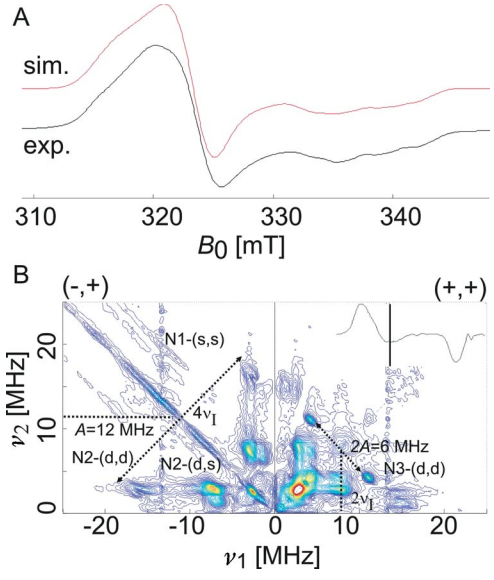

Figure 6. (A) X-band (9.5315 GHz) CW EPR spectra of **15** measured at 120 K in thf, experimental (exp.) and simulated (sim.). The simulation requires the g-matrix and N1, N2, and Ir hyperfine couplings. (B) Q-band (35.25 GHz) HYSCORE spectra of **15** in thf measured at 15 K at B_0 = 1200.0 mT. Selected crosspeaks are assigned to nitrogen N1, N2, and N3 with labels for nitrogen double-quantum (d) and single-quantum (s) frequencies. Inset: Q-band echo-detected EPR spectrum (first derivative) showing the observer position used to record the HYSCORE spectrum.

Reactivity

In accord with the electronic structure, the complexes [Rh(trop$_2$N$^{\cdot}$)(bipy)]OTf (**H**) and [M(trop$_2$N$^{\cdot}$)(phen)]OTf (**14a**: M = Rh; **15**: M = Ir) behave like aminyl radical complexes. In view of their almost-identical EPR spectra, it is not surprising that bipy complex **H** and phenanthrolin complexes **14a** and **15** show almost the same reactivity (Scheme 6).

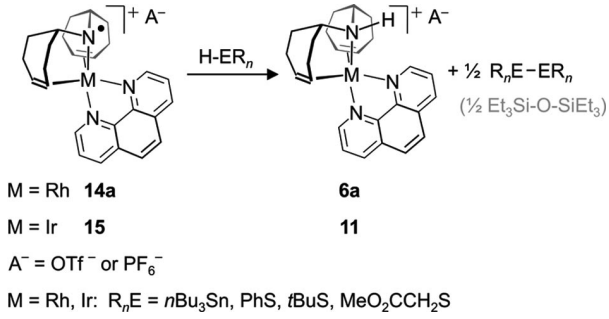

Scheme 6. Reactivity of **14a** and **15** with H atom donors. The reaction between **15** and Et$_3$SiH gives the siloxane (Et$_3$Si)$_2$O, which is shown in grey.

With hydrogen donors of a lower BDE than 360 kcal mol^{-1}, like tributylstannane (BDE = 308.5 kJ mol^{-1}) or thiophenol (BDE = 348.7 kJ mol^{-1}), very clean and fast reactions to amine complexes **6a** or **11** were observed. The H abstractions with the *tert*-butyl thiol or thioglycolic acid methyl ester (estimated BDE > 380 kJ mol^{-1}) are slightly endothermic and slower, but they are driven by the formation of the corresponding disulfides, which make the overall process strongly exothermic by ca. 300 kJ mol^{-1}.[24] Phenol does not react because of the strength of the O–H bond (BDE > 376 kJ mol^{-1}) and the instability of the peroxide, Ph–O–O–Ph. Although the reactions with silanes (BDE ≈ 360 kJ mol^{-1}), phenyl-substituted methanes (BDE < 350 kJ mol^{-1}), or 9,10-dihydroanthracene (BDE = 315.1 kJ mol^{-1}) are thermodynamically favored, no reaction was observed with rhodium complex **14a**

indicating a kinetic barrier for the H-abstraction reactions. As noted above, the iridium complex [Ir(trop$_2$N$^{\cdot}$)(phen)]-OTf (**15**) behaves slightly differently. This complex is highly unstable in thf solution and gives cleanly within seconds at room temperature amine complex **11**. When aminyl complex **15** is generated in the presence of 9,10-dihydroanthracene as H-donor, the expected anthracene is not observed although amine complex **11** was cleanly obtained. We were unable to determine the source of hydrogen that generates **11** from **15**.[25] Whereas rhodium complex **14a** remains unaffected in the presence of silane, iridium aminyl complex **15** does react rapidly with Et_3SiH (BDE = 377 kJ mol^{-1}) to form **11** and siloxane $Et_3Si–O–SiEt_3$ [δ(^{29}Si) = 9.1 ppm].[26] It is at present unclear by which mechanism the siloxane was formed.

Conclusions

Straight-forward simple routes to fivefold-coordinated 18-electron rhodium and iridium amine diolefin complexes were developed from readily available starting materials. Especially the acetonitrile complexes [Rh(trop$_2$NH)(MeCN)$_2$]-OTf (**5**) and [IrCl(trop$_2$NH)(MeCN)] (**10**) proved to be suitable precursor complexes for the syntheses of various phenanthroline-type complexes [M(trop$_2$NH)(R,R-phen)]$^+$ (**6a–d**, **11**; M = Rh$^{\mathrm{I}}$ or Ir$^{\mathrm{I}}$; R = substituents at phen). These complexes are quantitatively (judged by ^{1}H NMR spectroscopy) deprotonated by one equivalent of KO*t*Bu to give the neutral amido complexes [M(trop$_2$N)(R,R-phen)] (**12a–c**, **13**). The pK_a of the amine complexes in dmso is in a narrow range between 18.2 and 19, and it is remarkably independent of the metal center. We attribute this to the fact that the olefin moieties are arranged in a perpendicular fashion with respect to the NH–M-axis. Hence, the M→L back bonding, which is certainly larger in the iridium complexes and stabilizes the amido complex,[16b] has only a negligible effect on the pK_a. The reversible redox potential of amido complexes **12a–c** and **13** lies likewise within a narrow range of –0.54 to –0.60 V (in dmso vs. Fc$^+$/Fc). The NH bond energies in all amine complexes are estimated to be about 360 kJ mol^{-1}. Whereas small bases rapidly deprotonate the amine complexes to the corresponding amido complexes, a sizeable kinetic barrier may be encountered with sterically demanding bases, as indicated by data obtained from the self-exchange reaction [Equation (4), vide supra].

A second complete set of structures for an amine (trop$_2$NH), amido (trop$_2$N), and aminyl radical (trop$_2$N$^{\cdot}$) complex could be obtained (**6a**, **12a**, **14a**), and some general structural features become apparent: (i) The amine and amido complexes have rather similar structures; noteworthy is the pyramidal coordination sphere around the nitrogen center in the amido complexes. (ii) The ligand in the *trans* position to the amido ligand is bonded at slightly longer distances than in the corresponding amine complexes indicating a stronger *trans* influence of the amido group. (iii) Upon oxidation of the amido complexes to the aminyl radical complexes, the Rh–N(trop$_2$) bond shortens significantly (≈14 pm) and the coordination sphere around N becomes trigonal planar. Both effects are in accord with the assumption that the electron is removed from a d(M)–p(N) antibonding orbital.

The EPR results in combination with our previous study including DFT calculations[8] bolster this picture. Although significant spin population (about 30%) is located at the metal center, about 60% resides on the nitrogen, which justifies the aminyl radical complex description, [M(trop$_2$N$^{\cdot}$)(phen)]$^+$ (M = Rh: **14a**, M = Ir: **15**). Moreover, hydrogen-abstraction reactions with stannanes and thiols, which give the amine complexes, show that these compounds show the expected reactivity of aminyl complexes. Like in the deprotonation reactions of the amine complexes, our first experiments indicate that sizeable kinetic barriers may be associated with these H-abstraction reactions, which may have steric and/or electronic origins. A puzzle to be solved remains the apparently higher instability (and reactivity) of the iridium complex [Ir(trop$_2$N$^{\cdot}$)(phen)]$^+$ (**15**), although its ground-state structure must be very similar to that of rhodium complex **14a**. We have no satisfying explanation for this phenomenon at present, but we note that iridium radical complexes seemingly show higher reactivity.[11,20] Whether this is eventually a property of a transition state on the reaction coordinate in H-abstraction reactions remains to be investigated.

Experimental Section

General Techniques: All manipulations of air- or moisture-sensitive compounds were performed with a standard vacuum line in flame-dried flasks under an atmosphere of argon. The argon was provided by PANGAS and further purified with an MBraun 100 HP gas purification system. Solvents were distilled under argon from sodium (toluene), sodium/benzophenone (thf, dimethoxyethane, diethyl ether), sodium/benzophenone/tetraglyme (*n*-hexane), sodium–potassium alloy (benzene), calcium hydride (dichloromethane, acetonitrile). Air-sensitive compounds were stored and weighed in a glove box (M Braun: lab master 130 or 150B-G). Reactions in small quantities were performed within a glove box.

Cyclic Voltammetric Investigations: CV spectra were recorded with a Princeton Applied Research potentiostat/galvanostat model 263A or model 283. The measurements were performed with an apparatus designed by Heinze et al.[27] Working electrode: planar platinum electrode (approximate surface area 0.785 mm^2); reference electrode: silver; counter electrode: platinum wire. At the end of each measurement, ferrocene was added as internal standard for calibration (–0.352 V vs. Ag/AgCl).

EPR: The S-band CW EPR spectra were measured with a home-built instrument with a home-built split-ring resonator. The temperature was controlled by a liquid helium cryostat from Oxford, Inc. Measurements used microwave (mw) power of 11 mW, a modulation amplitude of 0.1 mT, and a modulation frequency of 100 kHz. The X-band CW EPR spectra were measured with a Bruker E500 spectrometer equipped with a liquid nitrogen cryostat by using a modulation amplitude of 0.2 mT and a modulation frequency of 100 kHz. The Q-band spectra were measured with a home-built instrument equipped with a liquid helium cryostat from

Oxford, Inc. The echo-detected EPR spectra were recorded at 15 K by using the two-pulse sequence $\pi/2$–τ–π–echo with $t_{\pi/2}$ = 50 ns, t_π = 100 ns, and a variable τ from 500 to 748 ns in 8 ns steps. Q-band HYSCORE spectra were measured at 15 K and a repetition rate of 1 kHz by using the sequence $\pi/2$–τ–$\pi/2$–t_1–π–t_2–$\pi/2$–τ–echo. The mw pulse lengths were t_π = 16 ns, $t_{\pi/2}$ = 16 ns, with starting times $t_{1,2}$ = 96 ns and a time increment $\Delta t_{1,2}$ = 12 ns. EPR data were simulated with the program EasySpin[28] and HYSCORE spectra with a program written in-house.[29]

UV/Vis: Spectra were recorded with a UV/Vis/NIR lambda 19 spectrometer in 5-mm quartz cuvettes (200–1000 nm). Time-dependent measurements were performed with an Analytik Jena Specord S100 (diode array) spectrometer.

NMR Spectra: NMR spectra were recorded with Bruker Avance 500, 300, or 250 spectrometers. The chemical shifts (δ) were measured according to IUPAC regulations and expressed in ppm relative to TMS and H_3PO_4 for ^1H, ^{13}C and ^{31}P, respectively.[30] Exception is for ^{103}Rh with the frequency reference Ξ = 3.16 MHz. Coupling constants J are given in Hertz [Hz] as absolute values, unless specifically stated. Where first-order analysis is appropriate, the multiplicity of the signals is indicated as s, d, t, q, or m for singlets, doublets, triplets, quartets, or multiplets, respectively. Otherwise, the spin systems are specified explicitly. The abbreviation br. is given for broadened signals. The benzylic protons and carbon atoms are designated as H^{bzl} and C^{bzl}, respectively, and the olefinic protons and carbon atoms as H^{ol} and C^{ol}, respectively. Only selected spectroscopic data of diagnostic value are given. For further details see the Supporting Information.

[Rh$_2$(μ-Cl)$_2$(trop$_2$NH)$_2$] (3): [Rh$_2$(μ$_2$-Cl)$_2$(cod)$_2$] (500 mg, 1.01 mmol) and trop$_2$NH (806 mg, 2.02 mmol, 2 equiv.) were dissolved in CH_2Cl_2 (20 mL). The bright orange-red solution turned dark red after 30 min, and the mixture was left overnight without stirring. Dark-red crystals were formed, which were isolated by filtration and washed with hexane. Drying in vacuo yielded an orange powder (874 mg, 78%). ^1H NMR (400.1 MHz, CD_2Cl_2): δ = 2.90 (s, 2 H, NH), 4.44 (s, 4 H, H^{bzl}), 5.97 (dd, $^3J_{HH}$ = 9.4 Hz, $^2J_{RhH}$ = 2.1 Hz, 4 H, H^{ol}), 6.20 (d, $^3J_{HH}$ = 9.4 Hz, 4 H, H^{ol}) ppm. ^{13}C NMR (100.6 MHz, CD_2Cl_2): δ = 71.4 [br. s, 8 C, C^{ol}], 73.1 (s, 4 C, C^{bzl}) ppm. ^{103}Rh NMR (12.7 MHz, CD_2Cl_2): δ = 2992 (s) ppm. ATR IR: $\tilde{\nu}$ = 3200 (w, NH stretch) cm^{-1}. UV/Vis (CH_3CN): λ (ε, L mol^{-1} cm^{-1}) = 232 (sh.), 289 (45700), 329 (sh.) nm. $C_{60}H_{46}Cl_2N_2Rh_2$ (1071.74): calcd. C 67.24, H 4.33, N 2.61, Cl 6.62; found C 67.03, H 4.47, N 2.89, Cl 6.77.

[Rh(trop$_2$NH)(MeCN)$_2$]OTf (5): To a solution of [Rh$_2$(μ-Cl)$_2$(trop$_2$NH)$_2$] (**3**; 100 mg, 93.4 μmol) in acetonitrile (25 mL) was added silver triflate (48 mg, 187 μmol, 2 equiv.). The mixture was heated at reflux overnight and after filtration through Celite all volatiles were removed in vacuo to give a yellow powder (134 mg, 98%). ^1H NMR (400.1 MHz, CD_3CN): δ = 2.37 (s, 3 H, axial-CH_3), 4.03 (s, 1 H, NH), 4.78 (s, 2 H, H^{bzl}), 5.36 (d, $^3J_{HH}$ = 9.4 Hz, 2 H, H^{ol}), 5.77 (dd, $^3J_{HH}$ = 9.4 Hz, $^2J_{RhH}$ = 2.5 Hz, 2 H, H^{ol}) (note: equatorial CH_3CN is exchanged for solvent molecules) ppm. ^{13}C NMR (100.6 MHz, CD_3CN): δ = 4.4 (s, 1 C, axial-CH_3), 70.3 (d, $^1J_{RhC}$ = 8.0 Hz, 2 C, C^{ol}), 71.0 (d, $^1J_{RhC}$ = 12.3 Hz, 2 C, C^{ol}), 71.6 (s, 2 C, C^{bzl}) ppm. ^{103}Rh NMR (12.7 MHz, CD_3CN): δ = 2311 (s) ppm. ATR IR: $\tilde{\nu}$ = 3131 (s, NH stretch), 2300 (w, C≡N stretch), 2280 (w, C≡N stretch) cm^{-1}. Raman: $\tilde{\nu}$ = 2297 (s, C≡N stretch), 2277(s, C≡N stretch) cm^{-1}. UV/Vis (CH_3CN): λ_{max} (ε, L mol^{-1} cm^{-1}) = 211 (55000), 229 (sh.), 284 (24.000), 320 (sh.) nm. $C_{35}H_{29}F_3N_3O_3RhS$ (731.59): calcd. C 57.46, H 4.00, N 5.74, S 4.38, F 7.79; found C 57.47, H 4.10, N 5.57, S 4.22, F 7.72.

[Rh(trop$_2$NH)(phen)]OTf (6a): To a solution of [Rh$_2$(μ-Cl)$_2$(trop$_2$NH)$_2$] (**3**; 300 mg, 0.28 mmol) in thf (100 mL) was added phenanthroline (114 mg, 0.62 mmol, 2.2 equiv.) and silver triflate (144 mg, 0.56 mmol, 2.0 equiv.), and the solution was heated at reflux overnight. The yellow suspension was filtered through Celite, and the residual silver chloride was washed with thf (30 mL). The filtrate was dried in vacuo and recrystallization from CH_2Cl_2/hexane (1:1) yielded the product as bright-orange needles (360 mg, 78%). Yellow crystals for X-ray structural analysis were grown from a concentrated thf/hexane (1:1) solution. ^1H NMR (500.2 MHz, [D$_6$]dmso): δ = 3.99 (d, $^3J_{HH}$ = 9.4 Hz, 2 H, H^{ol}), 4.94 (s, 2 H, H^{bzl}), 5.04 (s, 1 H, NH), 5.56 (d, $^3J_{HH}$ = 9.0 Hz, 2 H, H^{ol}) ppm. ^{13}C NMR (100.6 MHz, [D$_6$]dmso): δ = 68.0 (d, $^1J_{RhC}$ = 7.3 Hz, 2 C, C^{ol}), 69.3 (d, $^1J_{RhC}$ = 12.3 Hz, 2 C, C^{ol}), 71.4 (s, 2 C, C^{bzl}) ppm. ^{103}Rh NMR (15.8 MHz, [D$_6$]dmso): δ = 2111 (s) ppm. ATR IR: $\tilde{\nu}$ = 3196 (w, N–H stretch) cm^{-1}. $C_{43}H_{31}F_3N_3O_3RhS$ (829.61): calcd. C 62.25, H 3.76, N 5.06; found C 62.31, H 3.81, N 5.02.

General Procedure (GP 1) for [Rh(trop$_2$NH)(R,R-phen)]OTf (6b–d): To a solution of [Rh(trop$_2$NH)(MeCN)$_2$]OTf (**5**) in thf (5 mM) was added the phenanthroline derivative in slight excess (1.2–1.4 equiv.). The solution was heated at reflux overnight and cooled to room temperature, and the solvent was removed in vacuo. The raw product was subsequently recrystallized from CH_2Cl_2/hexane (1:1).

[Rh(trop$_2$NH)(4,7-Me$_2$-phen)]OTf (6b): Compound **5** (100 mg, 0.14 mmol) was treated with 4,7-dimethylphenanthroline (35.0 mg, 0.17 mmol) according to GP 1 to give a yellow powder (99 mg, 82%). ^1H NMR (400.1 MHz, CD_3CN): δ = 2.87 (s, 3 H, CH_3), 3.00 (s, 3 H, CH_3), 3.79 (s, 1 H, NH), 4.04 (dd, $^3J_{HH}$ = 9.5 Hz, $^2J_{RhH}$ = 1.0 Hz, 2 H, H^{ol}), 4.96 (s, 2 H, H^{bzl}), 5.50 (dd, $^3J_{HH}$ = 9.3 Hz, $^2J_{RhH}$ = 2.2 Hz, 2 H, H^{ol}) ppm. ^{13}C NMR (100.6 MHz, CD_3CN): δ = 18.5 (s, 1 C, CH_3), 18.7 (s, 1 C, CH_3), 67.9 (d, $^1J_{RhC}$ = 7.7 Hz, 2 C, C^{ol}), 69.2 (d, $^1J_{RhC}$ = 12.3 Hz, 2 C, C^{ol}), 71.5 (s, 2 C, C^{bzl}) ppm. ^{103}Rh NMR (12.7 MHz, CD_3CN): δ = 2099 (s) ppm. ATR IR: $\tilde{\nu}$ = 3221 (w, NH stretch) cm^{-1}.

[Rh(trop$_2$NH)(4,7-Ph$_2$-phen)]OTf (6c): Compound **5** (100 mg, 0.14 mmol) was treated with and 4,7-diphenylphenanthroline (64.0 mg, 0.19 mmol) according to GP 1 to give a bright-orange powder (96 mg, 71%). Bright-orange crystals for X-ray structural analysis were grown from a concentrated CH_2Cl_2 solution. ^1H NMR (400.1 MHz, [D$_6$]dmso): δ = 4.13 (d, $^3J_{HH}$ = 9.6 Hz, 2 H, H^{ol}), 4.96 (s, 2 H, H^{bzl}), 5.17 (s, 1 H, NH), 5.59 (dd, $^3J_{HH}$ = 9.6 Hz, $^2J_{RhH}$ = 2.2 Hz, 2 H, H^{ol}) ppm. ^{13}C NMR (75.5 MHz, [D$_6$]dmso): δ = 67.6 (d, $^1J_{RhC}$ = 8.5 Hz, 2 C, C^{ol}), 69.1 (d, $^1J_{RhC}$ = 12.8 Hz, 2 C, C^{ol}), 71.0 (s, 2 C, C^{bzl}) ppm. ^{103}Rh NMR (12.6 MHz, [D$_6$]dmso): δ = 2096 (s) ppm.

[Rh(trop$_2$NH)(5,6-Me$_2$-phen)]OTf (6d): Compound **5** (50 mg, 64 mmol) was treated with 5,6-dimethylphenanthroline (20 mg, 96 mmol) according to GP 1 to give a yellow powder (46 mg, 79%). Yellow crystals for X-ray structural analysis were grown from a concentrated CH_3CN solution. ^1H NMR (400.1 MHz, CD_3CN): δ = 2.86 (s, 3 H, CH_3), 2.89 (s, 3 H, CH_3), 3.83 (s, 1 H, NH), 4.07 (d, $^3J_{HH}$ = 9.3 Hz, 2 H, H^{ol}), 4.98 (s, 2 H, H^{bzl}), 5.54 (dd, $^3J_{HH}$ = 9.5 Hz, $^2J_{RhH}$ = 2.2 Hz, 2 H, H^{ol}) ppm. ^{13}C NMR (100.6 MHz, CD_3CN): δ = 15.1 (s, 1 C, CH_3), 15.2 (s, 1 C, CH_3), 68.0 (d, $^1J_{RhC}$ = 8.2 Hz, 2 C, C^{ol}), 69.5 (d, $^1J_{RhC}$ = 12.8 Hz, 2 C, C^{ol}), 71.5 (s, 2 C, C^{bzl}) ppm. ^{103}Rh NMR (12.6 MHz, CD_3CN): δ = 2093 (s) ppm. ATR IR: $\tilde{\nu}$ = 3198 (w, NH stretch) cm^{-1}.

[Rh(trop$_2$NH)(acac)] (7): To a solution of [Rh$_2$(μ-Cl)$_2$(trop$_2$NH)$_2$] (**3**; 250 mg 0.23 mmol) in thf (100 mL) was added a solution (0.5 mL) prepared from acetylacetone (1.05 mL, 10.2 mmol) and

KO*t*Bu (1.26 g 11.2 mmol) in methanol (10 mL). The yellow solution was heated at reflux overnight and cooled to room temperature, and the solvent was removed in vacuo. The raw product was recrystallized from CH_2Cl_2/hexane (1:1) to give a yellow crystalline solid (226 mg, 82%). Yellow crystals for X-ray structural analysis were grown from a concentrated CH_2Cl_2/hexane (1:1) solution. ^{1}H NMR (300.1 MHz, $CDCl_3$): δ = 1.65 (s, 3 H, CH_3), 1.90 (s, 3 H, CH_3), 2.92 (s, 1 H, NH), 4.40 (s, 2 H, H^{bzl}), 4.83 (d, $^3J_{HH}$ = 9.3 Hz, 2 H, H^{ol}), 5.38 (dd, $^3J_{HH}$ = 9.3 Hz, $^2J_{RhH}$ = 2.5 Hz, 2 H, H^{ol}) ppm. ^{13}C NMR (75.5 MHz, $CDCl_3$): δ = 27.8 (s, 1 C, CH_3), 28.7 (s, 1 C, CH_3), 66.8 (d, $^1J_{RhC}$ = 13.4 Hz, 2 C, C^{ol}), 69.9 (d, $^1J_{RhC}$ = 8.5 Hz, 2 C, C^{ol}), 73.0 (s, 2 H, C^{bzl}) ppm. ^{103}Rh NMR (12.7 MHz, $CDCl_3$): δ = 2998 (s) ppm. ATR IR: $\tilde{\nu}$ = 3063 (w, NH stretch) cm^{-1}. $C_{35}H_{30}NO_2Rh{\cdot}CH_2Cl_2$ (684.455): calcd. C 63.17, H 4.71, N 2.34; found C 62.94, H 4.79, N 2.00.

[Ir$_2$(μ-Cl)$_2$(trop$_2$NH)$_2$] (9): To a suspension of $[Ir_2(\mu_2\text{-}Cl)_2(coe)_4]$ (1.00 g, 1.11 mmol) in toluene (200 mL) was added trop$_2$NH (**2**; 887 mg 2.23 mmol), and the reaction mixture was heated at reflux for 48 h. A yellow suspension formed. The product was isolated by filtration, and it was then subsequently washed with toluene to give a yellow microcrystalline solid (809 mg, 58%). ^{1}H NMR (300.1 MHz, $CDCl_3$): δ = 3.67 (s, 2 H, NH), 4.58 (s, 4 H, H^{bzl}), 5.58 (d, $^3J_{HH}$ = 8.8 Hz, 4 H, H^{ol}), 5.83 (d, $^3J_{HH}$ = 9.1 Hz, 4 H, H^{ol}) ppm. ^{13}C NMR (75.5 MHz, [D$_6$]dmso): δ = 51.1 (s, 2 C, C^{ol}), 52.6 (s, 2 C, C^{ol}), 70.0 (s, 4 C, C^{bzl}) ppm. ATR IR: $\tilde{\nu}$ = 3199 (w, N–H stretch) cm^{-1}. $C_{60}H_{46}Cl_2Ir_2N_2$ (1250.36): calcd. C 63.17, H 4.71, N 2.34; found C 62.94, H 4.79, N 2.00.

[IrCl(MeCN)(trop$_2$NH)] (10): $[Ir_2(\mu\text{-}Cl)_2(trop_2NH)_2]$ (**9**; 500 mg, 0.4 mmol) was suspended in CH_3CN (75 mL), and the mixture was heated at reflux overnight whereby a white suspension formed. The reaction mixture was cooled to room temperature and all volatiles were removed in vacuo to yield a white flaky solid (515 mg, 97%). ^{1}H NMR (500.1 MHz, $CDCl_3$): δ = 2.50 (s, 3 H, CH_3), 4.40 (s, 1 H, NH), 4.48 (d, $^3J_{HH}$ = 8.7 Hz, 2 H, H^{ol}), 4.67 (s, 2 H, H^{bzl}), 5.00 (d, $^3J_{HH}$ = 8.7 Hz, 2 H, H^{ol}) ppm. ^{13}C NMR (125.8 MHz, $CDCl_3$): δ = 4.2 (s, 1 C, CH_3), 45.6 (s, 2 C, C^{ol}), 53.7 (s, 2 C, C^{ol}), 72.7 (s, 2 C, C^{bzl}) ppm.

[Ir(trop$_2$NH)(phen)]PF$_6$ (11): Complex **10** (250 mg, 0.38 mmol), phenanthroline (70.0 mg, 0.38 mmol, 1 equiv.), and $TlPF_6$ (160 mg, 0.46 mmol, 1.2 equiv.) were dissolved in chlorobenzene (10 mL). The dark-red solution was heated at reflux overnight, which resulted in the formation of a bright-orange suspension. The product was filtered and washed with ice-cold chlorobenzene to give a yellow powder (330 mg, 96%). ^{1}H NMR (300.1 MHz, [D$_8$]thf): δ = 3.26 (d, $^3J_{HH}$ = 8.8 Hz, 2 H, H^{ol}), 4.78 (s, 1 H, NH), 5.18 (d, $^3J_{HH}$ = 9.3 Hz, 2 H, H^{ol}), 5.36 (s, 2 H, H^{bzl}) ppm. ^{13}C NMR (62.9 MHz, [D$_6$]dmso): δ = 47.9 (s, 2 C, C^{ol}), 51.1 (s, 2 C, C^{ol}), 71.0 (s, 2 C, C^{bzl}) ppm. ATR IR: $\tilde{\nu}$ = 3233 (w, N–H stretch) cm^{-1}.

General Procedure (GP 2) for the Amido Complexes [Rh(trop$_2$N)-(R,R-phen)] (12a–c): To a solution of the amine complex in thf (18 mm) was added KO*t*Bu (1.0 equiv.). The volume of the solution was reduced to about 20%. *n*-Hexane was added slowly to reach a 1:1 (by vol.) mixture whereby the product precipitated. The product was filtered off and washed with *n*-hexane.

[Rh(trop$_2$N)(phen)] (12a): Complex **6a** (150 mg, 0.18 mmol) was treated with KO*t*Bu (21 mg, 0.18 mmol) according to GP 2 to give a dark-red powder (103 mg, 84%). Dark-red crystals for X-ray structural analysis were slowly grown from a concentrated thf solution. ^{1}H NMR (300.1 MHz, [D$_8$]thf): δ = 2.73 (d, $^3J_{HH}$ = 9.1 Hz, 2 H, H^{ol}), 4.30 (s, 2 H, H^{bzl}), 4.81 (d, $^3J_{HH}$ = 9.1 Hz, 2 H, H^{ol}) ppm. ^{13}C NMR (62.9 MHz, [D$_8$]thf): δ = 63.3 (d, $^1J_{RhC}$ = 13.0 Hz, 2 C, C^{ol}), 64.1 (2 C, C^{ol}; doublet not resolved due to overlapping solvent signals), 77.5 (s, C^{bzl}) ppm. ^{103}Rh NMR (12.7 MHz, [D$_8$]-thf): δ = 1570 (s) ppm. UV/Vis (thf): λ_{max} = 326 nm.

[Rh(trop$_2$N)(4,7-Me$_2$-phen)] (12b): Complex **6b** (120 mg, 0.14 mmol) was treated with KO*t*Bu (16 mg, 0.14 mmol) according to GP 2 to yield a brown powder (89 mg, 90%). ^{1}H NMR (250.1 MHz, [D$_8$]thf): δ = 2.76 (s, 3 H, CH_3), 2.95 (s, 3 H, CH_3), 3.45 (d, $^3J_{HH}$ = 9.5 Hz, 2 H, H^{ol}), 4.10 (s, 2 H, H^{bzl}), 5.01 (dd, $^3J_{HH}$ = 9.1 Hz, $^2J_{RhH}$ = 2.0 Hz, 2 H, H^{ol}) ppm. ^{13}C NMR (62.9 MHz, [D$_8$]thf): δ = 17.6 (s, 2 C, CH_3), 17.8 (s, 2 C, CH_3), 67.3 (s, 2 C, C^{ol}), 79.4 (s, 2 C, C^{bzl}) ppm. ^{103}Rh NMR (15.8 MHz, [D$_6$]-dmso): δ = 1547 (s) ppm.

[Rh(trop$_2$N)(4,7-Ph$_2$-phen)] (12c): Complex **6c** (100 mg, 0.10 mmol) was treated with KO*t*Bu (13 mg, 0.10 mmol) according to GP 2 to yield a dark red-brown powder (70 mg, 82%). ^{1}H NMR (250.1 MHz, [D$_6$]dmso): δ = 3.55 (d, $^3J_{HH}$ = 9.3 Hz, 2 H, H^{ol}), 4.10 (s, 2 H, H^{bzl}), 5.12 (d, $^3J_{HH}$ = 9.3 Hz, $^2J_{RhH}$ = 1.6 Hz, 2 H, H^{ol}) ppm. ^{13}C NMR (100.6 MHz, [D$_6$]dmso): δ = 65.3 (s, 2 C, C^{ol}), 66.9 (s, 2 C, C^{ol}), 78.9 (s, 2 C, C^{bzl}) ppm. ^{103}Rh NMR (15.8 MHz, [D$_6$]-dmso): δ = 1562 (s) ppm.

[Ir(trop$_2$N)(phen)] (13): To a solution of complex **11** (100 mg, 0.11 mmol) in thf (4 mL) was added KO*t*Bu (20 mg, 0.18 mmol, 1.6 equiv.) in one portion. An immediate color change from yellow to very dark green was observed. The volume of the solution was reduced to approx. 1 mL and then hexane (3 mL) was added. A green-brown powder precipitated, which was filtered and washed with hexane to yield a green-brown powder (70 mg, 83%). ^{1}H NMR (300.1 MHz, [D$_8$]thf): δ = 2.72 (d, $^3J_{HH}$ = 8.8 Hz, 2 H, H^{ol}), 4.30 (s, 2 H, H^{bzl}), 4.81 (d, $^3J_{HH}$ = 9.1 Hz, 2 H, H^{ol}) ppm. ^{13}C NMR (62.9 MHz, [D$_6$]dmso): δ = 44.0 (s, 2 C, C^{ol}), 50.8 (s, 2 C, C^{ol}), 77.0 (s, 2 C, C^{bzl}) ppm.

[Rh(trop$_2$N$^{\cdot}$)(phen)]OTf (14a): To a solution of amide **12a** (50 mg, 74 μmol) in thf (8 mL) was added ferrocenium triflate (25 mg, 74 μmol, 1 equiv.) in one portion. The volume of the solution was reduced to about 4 mL and hexane (4 mL) was then added whereupon a dark-green precipitate was formed. The product was filtered, washed with hexane (4 mL) and thoroughly dried in vacuo to afford radical **14a** as a finely divided pale-green powder. Dark-red crystals for X-ray structural analysis were grown from a saturated thf solution. UV/Vis (thf): λ_{max} = 217, 230, 267, 297 nm.

[Rh(trop$_2$N$^{\cdot}$)(4,7-Me$_2$-phen)]OTf (14b): To a solution of amide **12b** (18 mg, 26 μmol) in thf (1 mL) was added ferrocenium triflate (8 mg, 24 μmol, 1 equiv.) in one portion. Hexane (1 mL) was added, whereupon a dark-green precipitate was formed. The product was filtered, washed with hexane (1 mL), and thoroughly dried in vacuo. Radical **14b** was obtained as a pale-green powder.

[Ir(trop$_2$N$^{\cdot}$)(phen)](OTf/PF$_6$) (15): Ferrocenium triflate (22 mg, 66 μmol) and nBu$_4$NPF$_6$ (774 mg, 2 mmol) were dissolved in thf (5 mL) and neutral amide complex **13** (10 mg, 13 μmol) was dissolved in thf (0.5 mL). An aliquot (0.1 mL) of each of these solutions were combined in an EPR tube and sealed off.

X-ray Crystallography: Crystals of **3** were grown from the mother liquor (CH_2Cl_2) overnight at the bottom of the flask and isolated by decantation. Crystals of **5** were grown from a concentrated CH_3CN solution. Yellow crystals of **7** suitable for analysis were grown from a concentrated CH_2Cl_2/hexane (1:1) solution. Crystals of **6a** were grown from a concentrated thf/hexane (1:1) solution. Crystals of **6d** were grown from a concentrated CH_3CN solution. Dark-red crystals of **12a** were grown from a saturated thf solution. Dark-red crystals of **14a** were slowly grown from a concentrated thf solution. To avoid quality degradation, most single crystals were mounted in perfluoropolyalkyl ether oil on top of a glass fiber and

then brought into the cold nitrogen stream of a low-temperature device so that the oil solidified. Data collection for the X-ray structure determinations were performed with SMART APEX platforms with graphite-monochromated Mo-K_α radiation (λ = 0.71073 Å). The reflex intensities were measured by CCD area detectors. The collected frames were processed with the proprietary software SAINT.[31] Solution and refinement of the structures was performed with SHELXS-97[32] and SHELXL-97,[33] respectively. The structures were solved by the Patterson-method and successive interpretation of the difference Fourier maps, followed by full-matrix least-squares refinement (against F^2). Moreover, an empirical absorption correction (SADABS[34]) was applied to all structures. All non-hydrogen atoms were refined with anisotropic displacement parameters except for of **14a** in which the incorporated thf molecules were refined isotropically, because of high disordering. The thf molecules (**14a**) and dichloromethane molecules (**7**) in the crystal lattice are slightly (**7**) or strongly (**14a**) disordered and a high number of restraints were used to achieve a satisfactory wR_2 value. Hydrogen atoms were placed in their idealized positions and allowed to ride on the respective carbon atoms. Upon convergence, the final Fourier difference map of the X-ray structures of **6a**,**d**, **7**, and **14a** showed no significant peaks. For **12a**, some residual electron density was located close to the heavy atom rhodium (≈0.65 Å) even when an absorption correction was applied. Associated crystallographic data and other experimental details are summarized in Tables 4 and 5.

Table 4. Crystal data and refinement for compounds **3**, **5**, and **7**.

	3·$(CH_2Cl_2)_2$	**5**	**7**·CH_2Cl_2
Empirical formula	$C_{60}H_{46}Cl_2N_2Rh_2{\cdot}3CH_2Cl_2$	$C_{35}H_{29}F_3N_3O_3RhS$	$C_{36}H_{32}Cl_2NO_2Rh$
Formula mass	666.22	731.58	684.44
Crystal system	triclinic	monoclinic	monoclinic
Space group	$P\bar{1}$	$P2_1/n$	$P2_1/n$
a [Å]	10.920(3)	8.819(1)	16.1605(10)
b [Å]	12.821(3)	32.691(4)	13.0108(8)
c [Å]	13.328(3)	11.023(1)	30.422(2)
α [°]	65.876(5)	90	90
β [°]	66.155(5)	103.379(4)	100.7000(10)
γ [°]	67.821(4)	90	90
V [Å^3]	1506.5(6)	3091.7(6)	6285.3(7)
Z	2	4	8
F(000)	670	1488	2800
Crystal size [mm]	0.27 × 0.15 × 0.14	0.41 × 0.34 × 0.28	0.35 × 0.32 × 0.05
$\rho_{calcd.}$ [g cm^{-3}]	1.469	1.572	1.447
μ [mm^{-1}]	0.943	0.680	0.746
T [K]	100(2)	293(2)	298(2)
Reflections collected	8460	19510	26087
Unique reflections	5120 [R(int) = 0.0285]	5271 [R(int) = 0.0681]	9015 [R(int) = 0.0601]
Flack parameter			
GOF on F^2	1.053	1.144	1.051
R_1, wR_2 [$I > 2\sigma(I)$]	0.0569, 0.1340	0.0524, 0.0825	0.0508, 0.1016
R_1, wR_2 (all data)	0.0823, 0.1453	0.0780, 0.0886	0.1031, 0.1195

Table 5. Crystal data and refinement for compounds **6a**,**d**, **12a**, and **14a**.

	6a	**6d**·CH_3CN	**12a**·2thf	**14a**·2thf
Empirical formula	$C_{86}H_{60}F_6N_6O_6Rh_2S_2$	$C_{47}H_{38}F_3N_4O_3RhS$	$C_{40}H_{36.80}N_{2.40}O_{1.60}Rh_{0.80}$	$C_{34}H_{30.67}F_2N_2O_{3.33}Rh_{0.67}S_{0.67}$
Formula mass	1657.34	898.78	659.05	648.59
Crystal system	monoclinic	orthorhombic	monoclinic	monoclinic
Space group	$P2_1/c$	$P2_12_12_1$	$P2_1/n$	$P2_1/n$
a [Å]	18.8761(11)	13.073(3)	14.0367(4)	13.6004(10)
b [Å]	14.6610(9)	15.114(4)	18.4891(6)	17.4667(13)
c [Å]	13.7651(8)	19.522(5)	14.6286(4)	19.7546(15)
α [°]	90	90	90	90
β [°]	110.233(1)	90	96.2090(10)	106.6330(10)
γ [°]	90	90	90	90
V [Å^3]	3574.3(4)	3857.3(18)	3774.23(19)	4496.4(6)
Z	2	4	5	6
F(000)	1684	1840	1712	2004
Crystal size [mm]	0.48 × 0.35 × 0.32	0.22 × 0.20 × 0.17	0.32 × 0.25 × 0.21	0.21 × 0.16 × 0.06
$\rho_{calcd.}$ [g cm^{-3}]	1.540	1.548	1.450	1.437
μ [mm^{-1}]	0.598	0.562	0.500	0.490
T [K]	200(2)	298(2)	150(2)	200(2)
Reflections collected	30835	31550	118008	35606
Unique reflections	8869 [R(int) = 0.0289]	7880 [R(int) = 0.0864]	26075 [R(int) = 0.0543]	9198 [R(int) = 0.0669]
Flack parameter		0.02(3)		
GOF on F^2	1.046	1.003	1.114	1.047
R_1, wR_2 [$I > 2\sigma(I)$]	0.0347, 0.0830	0.0439, 0.0818	0.0619, 0.1207	0.0529, 0.1145
R_1, wR_2 (all data)	0.0414, 0.0865	0.0815, 0.0933	0.0865, 0.1292	0.1033, 0.1346

CCDC-679134 (for **3**), -679133 (for **5**), -673814 (for **7**), -673467 (for **6a**), -673466 (for **6d**), -673468 (for **12a**), and -673465 (for **14a**) contain the supplementary crystallographic data for this paper. These data can be obtained free of charge from The Cambridge Crystallographic Data Centre via www.ccdc.cam.ac.uk/data_request/cif.

Supporting Information (see footnote on the first page of this article): Detailed synthetic protocols and NMR spectroscopic data of compounds **3**, **5**, **6a**–**d**, **7**, **9**–**11**, **12a**–**c**, **13**, **14a**,**b**, and **15**; CW EPR spectra of [Rh(trop$_2$N$^{\cdot}$)(phen)]OTf at X-band.

Acknowledgments

This work was supported by the ETH Zürich and the Swiss National Science Foundation (SNF). H. G. and H. S. thank the Morgan Motor Company for continuous inspiration.

[1] For selected recent reports, see: a) J. Laleveé, D. Gigmes, D. Bertin, B. Graff, X. Allonas, J. P. Fouassier, *Chem. Phys. Lett.* **2007**, *438*, 346; b) F. Liu, K. Liu, X. Yuan, C. Li, *J. Org. Chem.*, DOI 10.1021/jo7015967 and references cited therein; c) K. Piech, T. Bally, A. Sikora, A. Marcinek, *J. Am. Chem. Soc.* **2007**, *129*, 3211; d) J. Guin, C. Mück-Lichtenfeld, S. Grimme, A. Studer, *J. Am. Chem. Soc.* **2007**, *129*, 4498 and references cited therein. Reviews: e) G. Merényi J. Lind in *N-Centered Radicals* (Ed.: Z. Alfassi), Wiley, New York, **1998**, pp. 599–613; f) B. J. Maxwell, J. Tsanaktsidis in *N-Centered Radicals* (Ed.: Z. Alfassi), Wiley, New York, **1998**, pp. 663–684.

[2] E. K. Barefield, M. T. Mocella, *J. Am. Chem. Soc.* **1975**, *97*, 4238.

[3] a) D. Sellmann, J. Müller, P. Hofmann, *Angew. Chem. Int. Ed. Engl.* **1982**, *21*, 691; b) D. Sellmann, J. Müller, *J. Organomet. Chem.* **1985**, *281*, 249; c) W. Kaim, R. Gross, *Angew. Chem. Int. Ed. Engl.* **1985**, *24*, 856.

[4] F. N. Penkert, T. Weyhermüller, E. Bill, P. Hildebrandt, S. Lecomte, K. Wieghardt, *J. Am. Chem. Soc.* **2000**, *122*, 9663.

[5] E. Kogut, H. L. Wiencko, L. Zhang, D. E. Cordeau, T. H. Warren, *J. Am. Chem. Soc.* **2005**, *127*, 11248.

[6] M. J. Ingleson, M. Pink, J. C. Huffman, H. Fan, K. G. Caulton, *Organometallics* **2006**, *25*, 1112–1119. The values given for the nitrogen hyperfine coupling (A = 0,0,160) G in this paper are unrealistic. The spin population was determined by DFT calculations.

[7] Y. Miyazato, T. Wada, J. T. Muckerman, E. Fujita, K. Tanaka, *Angew. Chem.* **2007**, *119*, 5830; *Angew. Chem. Int. Ed.* **2007**, *46*, 5728.

[8] T. Büttner, J. Geier, G. Frison, J. Harmer, C. Calle, A. Schweiger, H. Grützmacher, *Science* **2005**, *307*, 235–238.

[9] P. Maire, M. Königsmann, A. Sreekanth, J. Harmer, A. Schweiger, H. Grützmacher, *J. Am. Chem. Soc.* **2006**, *128*, 6578.

[10] Y. Mityazato, T. Wada, K. Tanaka, *Bull. Chem. Soc. Jpn.* **2006**, *79*, 745.

[11] a) M. Königsmann, N. Donati, J. Harmer, A. Sreekanth, H. Grützmacher, *Angew. Chem.* **2007**, *119*, 3637; *Angew. Chem. Int. Ed.* **2007**, *46*, 3567; b) N. Donati, M. Königsmann, D. Stein, L. Udino, H. Grützmacher, *Comptes Rendus Acad. Sci.* **2007**, *10*, 721–730.

[12] Various cationic [Rh(trop$_2$NH)(PR$_3$)]$^+$ complexes: a) P. Maire, T. Büttner, F. Breher, P. Le Floch, H. Grützmacher, *Angew. Chem.* **2005**, *117*, 6477; *Angew. Chem. Int. Ed.* **2005**, *44*, 6318; b) T. Zweifel, J.-V. Naubron, T. Büttner, T. Ott, H. Grützmacher, *Angew. Chem.* **2008**, *120*, 3289; *Angew. Chem. Int. Ed.* **2008**, *47*, 3245.

[13] T. Büttner, F. Breher, H. Grützmacher, *Chem. Commun.* **2004**, 2820–2821.

[14] It is well established that the equatorial position in TBP 18-electron complexes is labile (see standard textbooks on organometallic chemistry). Furthermore, for electronic reasons π-acceptor ligands bind in the equatorial position, whereas σ-donor ligands reside in the axial position of TBP; for a classical paper, see: A. Rossi, R. Hoffmann, *Inorg. Chem.* **1975**, *14*, 365.

[15] F. G. Bordwell, *Acc. Chem. Res.* **1988**, *21*, 456. For an extensive listing of pK_a values of various acids see: D. A. Ripin, D. A. Evans, http://evans.harvard.edu/pdf/evans_pKa_Table.pdf.

[16] a) P. Maire, F. Breher, H. Schönberg, H. Grützmacher, *Organometallics* **2005**, *24*, 3207; b) P. Maire, F. Breher, H. Grützmacher, *Angew. Chem.* **2005**, *117*, 6483; *Angew. Chem. Int. Ed.* **2005**, *44*, 6325.

[17] a) A. D. Bain, G. J. Duns, *Can. J. Chem.* **1996**, *74*, 819; b) A. D. Bain, http://www.chemistry.mcmaster.ca/~bain/exchange.html.

[18] T. Büttner, *Synthesis and Reactivity of Penta Coordinated Rhodium Amine-Diolefin Complexes*, ETH dissertation No. 15503, **2004**. Available through the internet under http://e-collection.ethbib.ethz.ch/show?type=diss&nr=15503.

[19] A. Vlcek, F. Baumann, W. Kaim, F. W. Grevels, F. Hartl, *J. Chem. Soc., Dalton Trans.* **1998**, 215.

[20] D. G. H. Hetterscheid, A. Koekkoek, H. Grützmacher, B. de Bruin, *Prog. Inorg. Chem.* **2007**, *55*, 249.

[21] a) W.-Z. Liu, F. G. Bordwell, *J. Org. Chem.* **1996**, *61*, 4778; b) F. G. Bordwell, J.-P. Cheng, J. John, A. Harrelson, *J. Am. Chem. Soc.* **1988**, *110*, 1229.

[22] A. Schweiger, G. Jeschke, *Principles of Pulse Electron Paramagnetic Resonance*, Oxford Press, Oxford, **2001**.

[23] A slight improvement in the simulation intensities is obtained by including a nuclear quadrupole coupling $|e^2qQ/h| \approx 30$ MHz.

[24] D. F. McMillen, D. M. Golden, *Ann. Rev. Phys. Chem.* **1982**, *33*, 493.

[25] Reactions in [D$_8$]thf also gave nondeuterated amine complex **11**. However, the rather acidic NH function easily exchanges with protic substances such that the eventually formed [Ir(trop$_2$ND)(phen)]$^+$ may have been converted into the NH complex with trace amounts of water.

[26] Et$_3$Si–O–SiEt$_3$ was identified by mass spectrometry and NMR spectroscopy [δ(^{29}Si) = 9.1 ppm]: a) R. L. Scholl, G. E. Maciel, W. K. Musker, *J. Am. Chem. Soc.* **1972**, *94*, 6376; b) R. K. Harris, B. J. Kimber, *Adv. Mol. Relax. Processes* **1976**, *8*, 15; c) E. I. Mysov, I. S. Akhrem, D. V. Avetisyan, *Org. Mass Spectrom.* **1976**, *11*, 358.

[27] K. Hinkelmann, J. Heinze, H. T. Schacht, J. S. Field, H. Vahrenkamp, *J. Am. Chem. Soc.* **1989**, *111*, 5078.

[28] S. Stoll, A. Schweiger, *J. Magn. Reson.* **2006**, *178*, 42; see http://www.esr.ethz.ch.

[29] Z. L. Madi, S. Van Doorslaer, A. Schweiger, *J. Magn. Reson.* **2002**, *154*, 181.

[30] R. K. Harris, E. D. Becker, S. M. Cabral de Menezes, R. Goodfellow, P. Granger, *Pure Appl. Chem.* **2001**, *73*, 1795–1818.

[31] *SAINT*, Reference manual, Siemens Energy and Automation, Madison, WI, **1994**–**1996**.

[32] G. M. Sheldrick, *SHELXS-97: Program for Crystal Structure Solution*, University of Göttingen, Germany, **1997**.

[33] G. M. Sheldrick, *SHELXL-97: Program for Crystal Structure Refinement*, University of Göttingen, Germany, **1997**.

[34] G. M. Sheldrick, *SADABS: Empirical Absorption Correction Program*, University of Göttingen, Germany, **1997**.

Received: July 16, 2008
Published Online: September 10, 2008

